

# Suzaku Discovery of Twin Thermal Plasma from the Tornado Nebula

Makoto SAWADA<sup>1</sup>, Takeshi Go TSURU<sup>1</sup>, Katsuji KOYAMA<sup>1</sup>, and Tomoharu OKA<sup>2</sup>

<sup>1</sup>*Department of Physics, Graduate School of Science, Kyoto University, Kitashirakawa Oiwake-cho, Sakyo-ku, Kyoto 606-8502  
sawada@cr.scphys.kyoto-u.ac.jp*

<sup>2</sup>*Department of Physics, Faculty of Science and Technology, Keio University, Hiyoshi, Kohoku-ku, Yokohama 223-8522*

(Received 2011 April 28; accepted 2011 May 20)

## Abstract

The Tornado nebula (G 357.7–0.1) is a mysterious radio source with bright “head” and faint “tail” located in the direction of the Galactic center (GC) region. We here report the discovery of two diffuse X-ray sources at the head and tail of the Tornado with the Suzaku satellite. We found emission lines from highly ionized atoms in the two sources. The spectra are reproduced by an optically thin thermal plasma with a common temperature of 0.6–0.7 keV. The interstellar absorption ( $N_{\text{H}}$ ) of these sources are the same and are slightly larger than that of the GC distance. Since the estimated distance using the  $N_{\text{H}}$  value is consistent with the radio observation of the Tornado, these X-ray sources are likely associated with the Tornado nebula. The twin-plasma morphology at the both ends of the Tornado suggests that the system is a bipolar/outflow source.

**Key words:** ISM: individual (G357.7–0.1)—ISM: jets and outflows—X-ray:ISM

## 1. Introduction

G 357.7–0.1 is a bright radio object near the Galactic center (GC) direction and was first catalogued by Mills et al. (1960) as MSH 17-39. The extended, non-thermal emission with the spectral index of  $\sim -0.6$  (Dickel et al. 1973, Slee & Dulk 1974) and the linear polarization of  $\lesssim 10\%$  (e.g. Kundu et al. 1974) placed this source as one of the Galactic supernova remnant (SNR).

It has an elongated shape with  $\sim 10'$  length and has the brightest peak offset to one side, which is called the “head”, while fainter emissions are elongated to the other side, called the “tail”. Unusual structure was found with the higher resolution observations. The remarkable feature is the several co-axial filamentary arcs swirling around its major axis, and hence nicknamed as the “Tornado nebula” (figure 1a: Shaver et al. 1985, Becker & Helfand 1985, Helfand & Becker 1985). Stewart et al. (1994) corrected the large-scale brightness gradient of the radio map, and found a bipolar radio structure along the major axis.

The distance to the Tornado is constrained to be  $> 6$  kpc from HI absorption measurements (Radhakrishnan et al. 1972). Recently, OH maser at 1720 MHz, supporting evidence for the shocked molecular clouds, is detected at the head (Frail et al. 1996, Yusef-Zadeh et al. 1999, Lazendic et al. 2004). From the velocity of the OH maser ( $-12.4$  km s<sup>-1</sup>), the distance is estimated to be 11.8 kpc (Frail et al. 1996). The H<sub>2</sub> emission lines are also detected toward the head of the Tornado (Lazendic et al. 2004).

The origin of the Tornado nebula has been controversial due to its peculiar appearance. Some scenarios are based on the head-tail structure; the center of activity is located at the brightest head and the tail is the periphery structure. The source may be either a radio galaxy

with one-sided jet (Weiler & Panagia 1980, Miley 1980), a Galactic nebula powered by a pulsar, or a Galactic binary source located at the head (Shaver et al. 1985, Becker & Helfand 1985, Shull et al. 1989).

The other scenarios are along the lines of bipolar-like structure: an extragalactic double-lobed source (Caswell et al. 1989), an exotic remnant by an equatorial supernova of a rotating massive star (Shaver et al. 1985), or precessing jets of binary accretion system (Shaver et al. 1985, Manchester 1987, Caswell et al. 1989). The problem of these scenarios is that no compact source has been found near at the center of the Tornado.

In the X-ray band, ASCA found a hint of weak X-rays from the Tornado (Yusef-Zadeh et al. 2003). Then Gaensler et al. (2003) discovered a diffuse X-ray source in the head with Chandra. From the centrally filled X-rays, the authors proposed that the Tornado is a Galactic mixed-morphology SNR (Rho & Petre 1998). However the nature of the X-rays, whether thermal or non-thermal, was not clear due to the limited photon statistics.

In order to give further constraint on the origin from the high energy phenomena, we conducted deep X-ray observations on the Tornado nebula with the X-ray Imaging Spectrometer (XIS: Koyama et al. 2007a) onboard Suzaku (Mitsuda et al. 2007). We present the discovery of twin thermal plasmas associated with the head and tail of the Tornado. We investigate possible interaction of the Tornado with molecular clouds by referring the data from the Nobeyama Radio Observatory (NRO) 45-m telescope. Based on these new results, we discuss the nature of the X-ray source.

Throughout this paper, east and west indicate for the direction in the Galactic longitude, and north and south for that in the Galactic latitude. Statistical uncertainties are represented by the 90% confidence intervals.

Table 1. Log of Suzaku observations of the Tornado

Sequence no.	Aim point		Start date	Effective exposure	Field name
	$\alpha$ (J2000.0)	$\delta$ (J2000.0)			
503015010	17 <sup>h</sup> 40 <sup>m</sup> 07 <sup>s</sup>	-30°57'45"	2008/9/19	56.8 ks	obs08
504036010	17 <sup>h</sup> 40 <sup>m</sup> 31 <sup>s</sup>	-30°56'56"	2009/8/29	125 ks	obs09

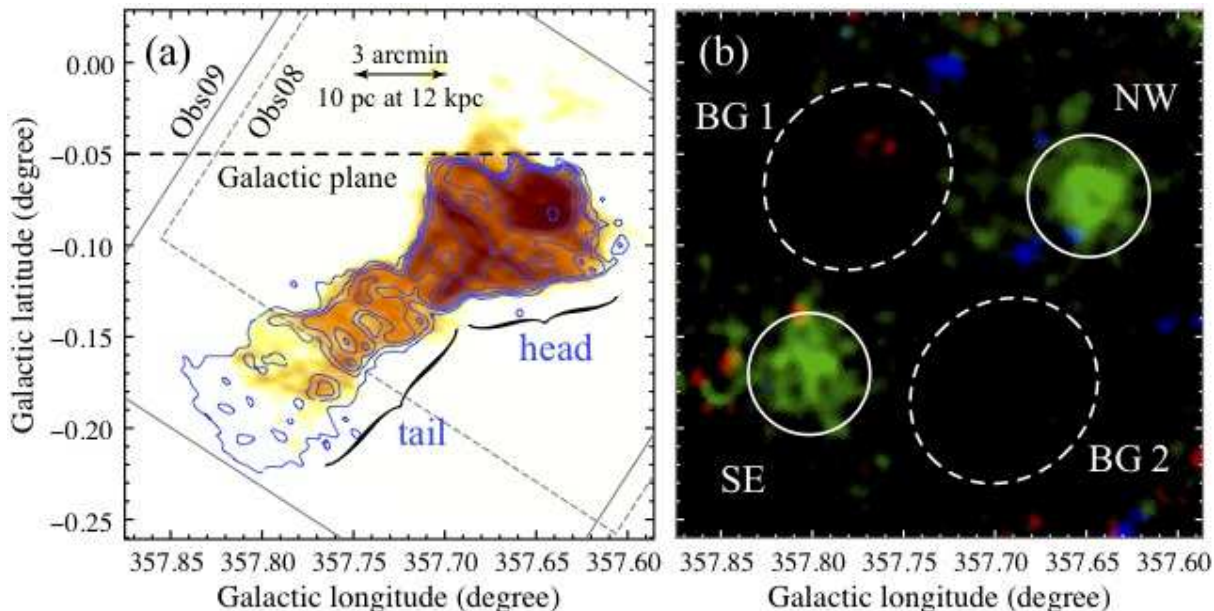


**Fig. 1.** (a) The 1.4 GHz radio continuum map from the Very Large Array data archives. Overlaid contours represent the radio map with the Australia Telescope Compact Array (ATCA) made by combining 4.79 and 5.84 GHz images (the fainter emission along the tail is enhanced; Stewart et al. 1994). The XIS fields of view are indicated with the solid and dashed rectangles. (b) Smoothed broad-band XIS images of the Tornado nebula: soft (0.5–1.5 keV in red), medium (1.5–3.0 keV in green), and hard (3.0–7.0 keV in blue) bands are displayed. The data from the three CCDs are merged, NXB are subtracted, and vignetting are corrected. The two fields are combined with normalization of the exposure times. Source and background extraction regions are shown with the solid and dashed ellipses, respectively.

## 2. Observations and Data Reduction

The Tornado nebula was observed twice. The first observation was centered at the head region, while the second covered the whole structure of the Tornado. The observation log is given in table 1.

The XIS consists of four CCD cameras each placed at the focal planes of four X-Ray Telescopes (XRTs: Serlemitsos et al. 2007). Three sensors employ Front-Illuminated (FI) CCDs (XIS0, 2, and 3) while the other employs a Back-Illuminated (BI) CCD (XIS1). XIS 2 has not been functional since an anomaly in 2006 November. The XIS is equipped with spaced-row charge injection technique (SCI: Bautz et al. 2004) to restore the radiation-induced degradation of the energy gain and resolution. The field of view (FOV) of XIS combined with XRT covers an  $18' \times 18'$  region with a pixel scale of  $1'' \text{ pixel}^{-1}$ . An angular resolution of  $1.9\text{--}2.3$  in the half-power diameter (HPD) is almost independent of photon energies and off-axis angles within  $\sim 10\%$ . The total effective area of operational XIS0, 1, and 3 with three XRTs is  $430 \text{ cm}^2$

at 8 keV. Due to the low orbital altitude of Suzaku at  $\sim 550 \text{ km}$ , the XIS achieves a low and stable background environment suitable for studying faint diffuse sources.

In the present observations, the XIS was operated in the normal clocking mode with the SCI technique. The data reduction was made from the pipeline processing version 2.4. We updated the gain correction method to be optimized for the SCI (Uchiyama et al. 2009) by using the makepi files version 20090915 provided by the XIS team. The systematic uncertainty in the energy scale is  $\lesssim 10 \text{ eV}$  at 5.9 keV. We removed events during the South Atlantic Anomaly passages and Earth night-time and day-time elevation angles below  $5^\circ$  and  $10^\circ$ , respectively. We also removed hot and flickering pixels. We reduced the data using the software packages HEADAS version 6.9.

## 3. Analysis and Results

In the spectral analysis, we used the Xspec (Arnaud 1996) version 12.5.1. The non-X-ray background (NXB) data were generated by xisnxbgen (Tawa et al. 2008).

The redistribution matrix function is generated by `xisrmfgen` and the auxiliary response function is made by a ray-tracing simulator `xissimarfgen` (Ishisaki et al. 2007).

### 3.1. X-ray Images

The NXB subtracted data were used to make the three-band X-ray images in the soft (0.5–1.5 keV), medium (1.5–3.0 keV), and hard (3.0–7.0 keV) bands. Figure 1b shows the results after the vignetting correction. We see two diffuse emissions only in the medium band (1.5–3.0 keV). We hereafter call these sources as “NW” and “SE”. The apparent sizes of NW and SE are  $\sim 4'$ , which are larger than the HPD of the Suzaku XRT ( $\sim 2'$ ). Thus these X-ray sources are not single point sources, but diffuse or ensemble of multiple point sources. We then searched for X-ray point sources in the source areas from the Chandra Catalog (Evans et al. 2010), and found only one Chandra point source in the SE area. The flux is only 0.7% of the total flux (after the background subtraction; see § 3.2 and § 3.3) in the SE area in the 1.2–7.0 keV band. We further made the X-ray light-curve from NW and SE areas, and found no time variability of these sources. Thus NW and SE must be extended sources.

### 3.2. Background Selection

The background X-rays in the source (NW and SE) areas are mainly due to the Galactic diffuse X-ray emission (GDXE), because the two sources are near the GC and the Galactic plane. The flux (surface brightness) of the GDXE smoothly decreases with increasing distances from the GC and the plane, while the spectrum shape has no significant position-to-position variation (e.g., Uchiyama et al. 2011). In order to investigate the flux and spectrum variation near the source fields, we select two background regions from the nearby blank sky (BG 1 and BG 2: broken ellipses in figure 1). Figure 2 shows the NXB-subtracted spectra of BG 1 and BG 2. We see that the over-all spectral structures and fluxes are very similar to each other.

For the quantitative study, we conducted spectral fittings with the following process. The GDXE is known to exhibit strong K-shell lines from highly ionized silicon (Si), sulfur (S), and iron (Fe) (Yamauchi & Koyama 1993). In fact, the XIS spectra of BG 1 and BG 2 clearly exhibit the highly ionized Si, S, and Fe K-shell lines. The co-existence of these lines indicates that the spectra require at least two temperature plasmas.

The previous studies on the GDXE near the GC direction (e.g., Muno et al. 2004, Ryu et al. 2009) showed that the GDXE spectra can be fitted with two plasmas in collisional ionization equilibrium (CIE): a low-temperature ( $kT \sim 1$  keV) CIE for the Si and S lines, and a high-temperature ( $kT \sim 6$  keV) CIE for the Fe line. We therefore apply a two-temperature CIE plasma model by using the `Apec` code (Smith et al. 2001). We also included a Gaussian in the GDXE as a  $K\alpha$  emission line at 6.40 keV from neutral irons (Fe I), which is also found in the GDXE (e.g., Koyama et al. 2007b). These three components are attenuated by interstellar extinction (Wabs: Morrison & McCammon 1983) toward the GC distance. Then, the

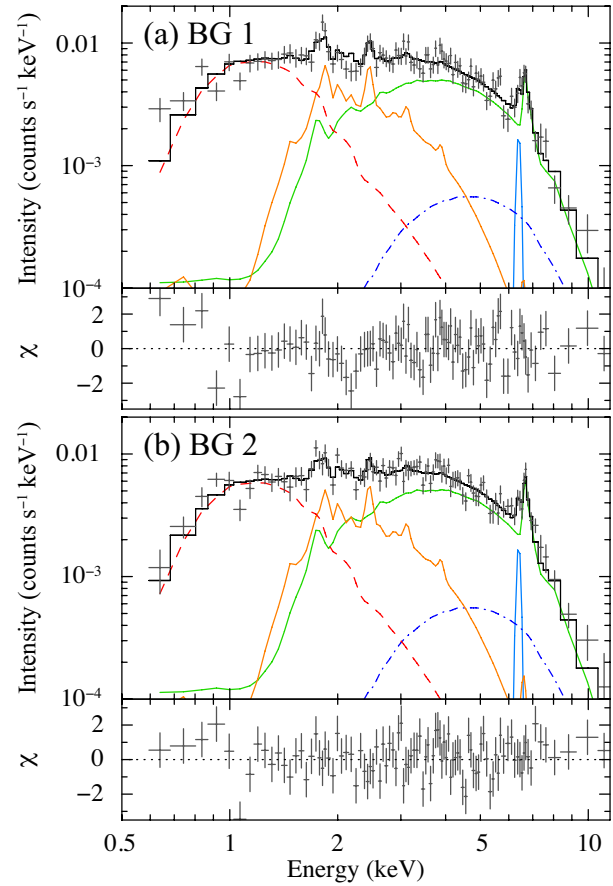


**Fig. 2.** (a) The NXB-subtracted spectra (gray crosses) and the best-fit models (black histograms) of BG 1. The difference of effective area between the two is corrected and only the results of FIs are shown for simplicity. The solid, dashed, and dash-dotted curves represent contributions from the GDXE, the foreground emission, and the CXB, respectively. (b) Same as panel (a), but for BG 2.

GDXE is written as:

$$\text{Wabs1} \times (\text{Apec1} + \text{Apec2} + \text{Gaussian}). \quad (1)$$

The temperatures ( $kT$ ), chemical abundance of metals ( $Z$ ) relative to the solar values (Anders & Grevesse 1989), the volume emission measures of the plasmas, the surface brightness of Fe I  $K\alpha$  line ( $S_{6.4}$ ), and the hydrogen-equivalent column density of the absorbing materials ( $N_H$ ) were free parameters.

As is seen in figure 2, the spectra of BG 1 and BG 2 exhibit significant emission in the soft band (0.5–1.5 keV). If these soft X-rays come from the GDXE, the X-rays should be heavily attenuated by interstellar extinction toward the GC distance. Therefore the soft X-rays are mainly foreground emissions. The soft X-rays are also observed near the GC region ( $|l| < 1^\circ$ ) by Ryu et al. (2009). They found that the soft X-ray emission is almost uniform within the central one degree on the plane. They applied the model below:

$$\text{Wabs2} \times \text{Apec3}. \quad (2)$$

Since the absolute Galactic latitude of the Tornado fields are close to that of the region of Ryu et al. (2009), we can reasonably assume that the typical parameters for the soft X-ray spectrum are same as those of Ryu et al. (2009): the plasma temperature of 0.9 keV, the chemical abundance<sup>1</sup> of  $5 \times 10^{-3} Z_{\odot}$ , and the hydrogen-equivalent absorption column of  $2.0 \times 10^{21} \text{ cm}^{-2}$ . Thus for the foreground soft X-ray spectrum, only the normalization was a free parameter.

The other background component, the Cosmic X-ray background (CXB), is isotropic and we adopted the empirical form, an absorbed power-law:

$$\text{Wabs}3 \times C \times (E/\text{keV})^{-\Gamma}, \quad (3)$$

where  $C$  is the normalization constant at 1 keV and  $\Gamma$  is the photon index of the power-law. These are fixed to be  $C = 7.4 \times 10^{-7} \text{ photons s}^{-1} \text{ cm}^{-2} \text{ arcmin}^{-2}$  and  $\Gamma = 1.486$  according to Kushino et al. (2002). Since the CXB should be absorbed by the interstellar materials throughout the whole Galaxy, we assumed the hydrogen-equivalent absorption column toward the CXB to be twice of that for the GDXE ( $N_{\text{H}}$ ).

In the model fitting, all the free parameters are allowed to be independent between the two regions, BG1 and BG2. The model fit was acceptable for both the spectra. The results are shown in figure 2 and the best-fit parameters are listed in table 2.

We found that the best-fit parameters for the GDXE components are all consistent between BG1 and BG2 within the statistical errors, and hence can assume that the background spectrum and flux are essentially constant near at the source areas. We therefore merged BG1 and

BG2 to increase statistics. The best-fit  $N_{\text{H}}$  for the merged spectrum is  $(5.3 \pm 0.4) \times 10^{22} \text{ cm}^{-2}$ .

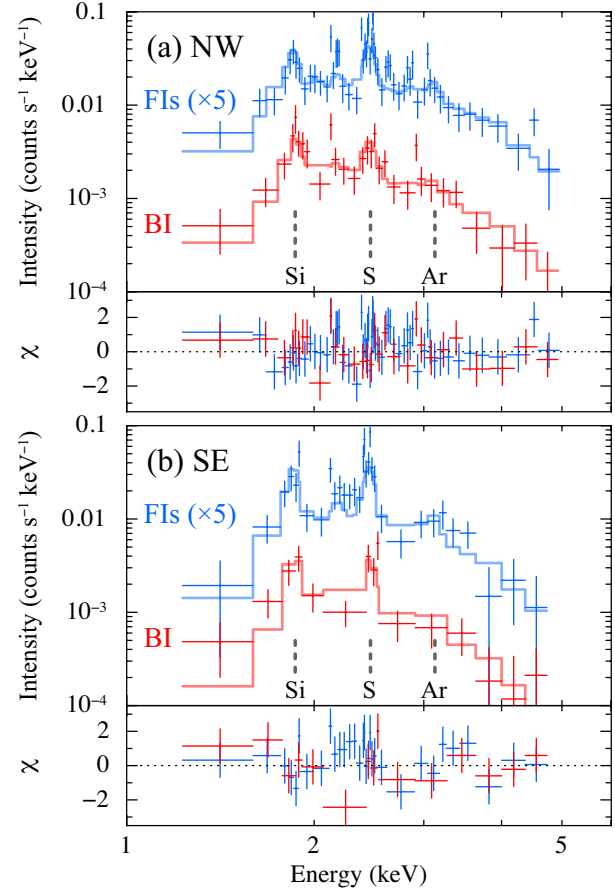


**Fig. 3.** (a) The background-subtracted spectra for NW. The FI and BI spectra are separately given by blue and red crosses, respectively. For visibility, the FI spectrum is multiplied by 5. The blue and red histograms are the best-fit model of FI and BI spectra, respectively. (b) Same as panel (a) but for SE.

<sup>1</sup> Since the true origin of the foreground emission is unknown at present, we applied a phenomenological model, which gives a reasonable fit to the data. Therefore apparent low abundances in this model should not be taken seriously.

**Table 2.** Best-fit parameters of the background emission.

Parameter	BG 1	BG 2
— Low temperature plasma —		
$kT$ (keV)	$0.90^{+0.17}_{-0.19}$	$0.96^{+0.22}_{-0.17}$
Norm*	$8.7^{+9.6}_{-3.4}$	$6.4^{+3.6}_{-2.6}$
— High temperature plasma —		
$kT$ (keV)	$6.5^{+1.3}_{-1.3}$	$6.5^{+1.2}_{-0.7}$
Norm*	$2.3^{+0.6}_{-0.4}$	$2.4^{+0.4}_{-0.3}$
— Common Parameters —		
$S_{6.4}^{\dagger}$	$3.8^{+1.8}_{-1.7}$	$3.8^{+1.6}_{-1.7}$
$Z$ ( $Z_{\odot}$ )	$0.53^{+0.16}_{-0.14}$	$0.58^{+0.15}_{-0.13}$
$N_{\text{H}}$ ( $10^{22} \text{ cm}^{-2}$ )	$5.2^{+0.8}_{-0.6}$	$5.3^{+0.6}_{-0.5}$
Foreground Norm*	$1.1^{+0.1}_{-0.1}$	$0.91^{+0.06}_{-0.06}$
$\chi^2/\text{d.o.f.}$	201/171	190/171

\* The normalized volume emission measure ( $VEM$ ) represented as  $10^{-7} \times \frac{VEM}{4\pi d^2 A} \text{ cm}^{-5} \text{ arcmin}^{-2}$ , where  $d$  and  $A$  are the distance and the solid angle of plasma, respectively.

<sup>†</sup> The average surface brightness in the unit of  $10^{-8} \text{ photons s}^{-1} \text{ cm}^{-2} \text{ arcmin}^{-2}$ .

**Table 3.** Best-fit parameters of the diffuse sources.

Parameter	NW	SE
$N_{\text{H}}$ ( $10^{22} \text{ cm}^{-2}$ )	$6.6^{+1.1}_{-0.8}$	$7.4^{+1.7}_{-1.4}$
$kT$ (keV)	$0.73^{+0.15}_{-0.15}$	$0.59^{+0.18}_{-0.15}$
$Z$ ( $Z_{\odot}$ )*	$0.89^{+0.37}_{-0.28}$	$1.7^{+1.3}_{-0.7}$
$S_{\text{X}}^{\dagger}$	$2.8^{+0.2}_{-0.2}$	$2.4^{+0.2}_{-0.2}$
$L_{\text{X}}^{\ddagger}$	$2.4^{+0.1}_{-0.1}$	$3.6^{+0.3}_{-0.3}$
$\chi^2/\text{d.o.f.}$	85/82	49/41

\* The chemical abundance of Si, S, and Ar relative to the solar values. The abundances of the other elements are fixed at the solar values.

<sup>†</sup> The average surface brightness in the unit of  $10^{-6} \text{ photons s}^{-1} \text{ cm}^{-2} \text{ arcmin}^{-2}$  in the 0.5–7.0 keV band.

<sup>‡</sup> The luminosity in the unit of  $10^{35} \text{ erg s}^{-1}$  in the 0.5–7.0 keV band. The absorption is corrected and the distances are assumed to be 12.0 kpc (see § 4.1).

### 3.3. Spectra of NW and SE

We extracted the spectra from the NW and SE regions (solid circles in figure 1b), then subtracted the NXB and merged-background spectra. Figure 3 shows the background-subtracted spectra of NW and SE. We clearly see several emission lines from highly ionized atoms, Si, S and argon (Ar). We therefore fitted the spectra with an optically thin thermal plasma model in CIE (Apec) absorbed by the interstellar medium (Wabs). Free parameters were the chemical abundances of Si, S, and Ar, the temperatures and normalization of the CIE plasma, and absorption ( $N_{\text{H}}$ ). The abundances of the elements other than Si, S, and Ar were fixed to the solar values. All the abundances in the absorbing materials were also fixed to be solar. With this model, we obtained satisfactory fits both for NW and SE (figure 3). The best-fit parameters are given in table 3.

## 4. Discussion

### 4.1. Nature of the X-ray Sources and Association to the Tornado

We find that the absorption column densities ( $N_{\text{H}}$ ) for the NW and SE sources are very similar to each other (table 3). Since the  $N_{\text{H}}$  values for the GDXE near the source region are almost constant at  $(5.3 \pm 0.4) \times 10^{22} \text{ cm}^{-2}$ , the same  $N_{\text{H}}$  values for NW and SE supports that the two sources are located at nearly the same distances.

Assuming that the distance of the GDXE is 8 kpc and that the interstellar gas density along the line-of-sight is constant, the distances of NW and SE can be estimated by the  $N_{\text{H}}$  ratio relative to the background emission of  $(5.3 \pm 0.4) \times 10^{22} \text{ cm}^{-2}$  as  $10.0^{+1.8}_{-1.4}$  and  $11.2^{+2.7}_{-2.3}$  kpc, respectively. These distances are almost consistent with the radio distance of the Tornado ( $\sim 12$  kpc; Frail et al. 1996). In the projected image, the radio emission of the Tornado appears to be associated with the two X-ray structures at the both ends (see figure 4). Thus we argue that the two X-ray sources are physically connected to the Tornado nebula.

The two diffuse sources are found to exhibit optically thin thermal nature. In fact, the X-ray emission from the sources are described with CIE plasmas of nearly the same temperatures (0.6–0.7 keV). The abundances are consistent with the solar values. This indicates that the X-ray emitting materials mainly consist of interstellar gas. If the distance of the Tornado is 12 kpc, the X-ray source size of  $4'$  corresponds to 14 pc. Assuming a spherical shape with uniform density, we derive the physical parameters of the NW and SE plasmas, electron density ( $n_e$ ), mass ( $M$ ) and total thermal energy ( $E_{\text{th}}$ ), as are listed in table 4.

We found no hint of non-thermal emission from the NW and SE sources. Assuming the photon index of 2, we obtained the  $3\text{-}\sigma$  upper limits of the luminosities of non-thermal X-rays to be 1.1% and 2.0% of those of the thermal plasmas in the 0.5–7.0 keV band for NW and SE, respectively.

**Table 4.** Physical parameters of the X-ray emitting plasma.

Parameter	NW	SE
$VEM (10^{58} \text{ cm}^{-3})^*$	1.0	1.5
$n_e (\text{cm}^{-3})$	0.49	0.59
$M (M_{\odot})$	23	29
$E_{\text{th}} (10^{49} \text{ erg})$	8.3	8.2

\* These values are taken from the best-fit model in table 3 at the distance of 12 kpc.

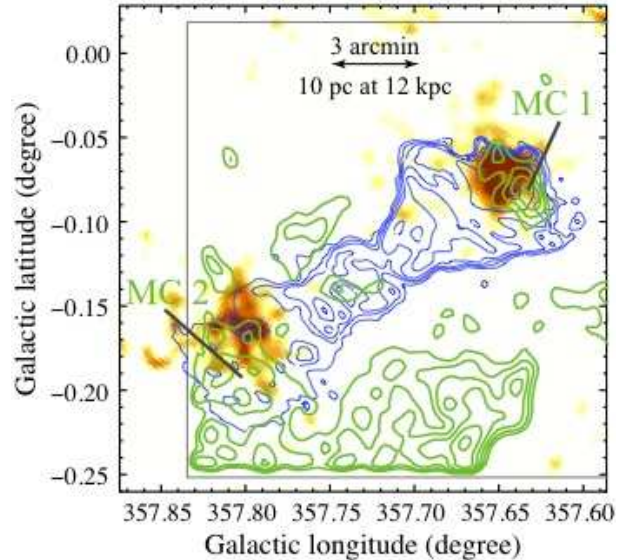


**Fig. 4.** Multi-wavelength image of the Tornado nebula: the medium band (1.5–3.0 keV) image overlaid with contours of the radio continuum emission with the ATCA (blue) and CO  $J=1-0$  ( $V_{\text{LSR}} = -11 \pm 1 \text{ km s}^{-1}$ ) with the NRO 45 m telescope (green). The FOV of the NRO observation is shown with the solid rectangle.

### 4.2. Bipolar Structure of the Tornado Nebula

The two X-ray plasmas are located at the both ends (head and tail) of the symmetric (bipolar-like) radio structure found by Stewart et al. (1994). Since the properties of the X-ray plasmas are almost identical, these would be the twins formed by a common process. A plausible scenario is that the X-ray plasmas have been generated by the termination shocks at the intersecting molecular clouds. In fact the shocked molecular cloud associated with the Tornado has been found near NW (Frail et al. 1996). To confirm the cloud interactions, we further search for the molecular structure near at the NW and SE regions using the data of CO  $J=1-0$  taken with the NRO 45-m telescope (private communication with T. Oka). The results in the velocity range of  $11 \pm 1 \text{ km s}^{-1}$ , close to the velocity of the OH maser near at NW, are shown in figure 4. We clearly see CO counterparts near NW (MC 1) and SE (MC 2).

As we described in § 1 (Introduction), many ideas for the origin of the Tornado have been proposed. The present result that the Tornado has bipolar X-rays at the head and tail excludes most of these scenarios. In the following sections (§ 4.3 and § 4.4), we discuss two plausible origins.

### 4.3. Bipolar Jet from a Binary Accretion System

One possibility is that the Tornado is made by bipolar jets from a binary accretion system. The filamentary radio arcs swirling around the major axis would be due to the precession of jets as is found in SS 433. The twin X-ray emitting plasmas are made by the shock with molecular clouds. Bipolar jets have usually a bright central power source, but no X-ray source is found from the center of the Tornado nebula. We set the 3- $\sigma$  upper limit on the luminosity to be  $1.9 \times 10^{33}$  erg s $^{-1}$  in the 0.5–10.0 keV band, assuming the absorption column of  $N_{\text{H}} = 7 \times 10^{22}$  cm $^{-2}$ , the power-law spectrum with the photon index of 2, and the distance of 12 kpc. Chandra has gave more severe constraint of  $\sim 1 \times 10^{33}$  erg s $^{-1}$  (Gaensler et al. 2003). These upper limits are only less than 1% of NW and SE luminosities of  $2.4 \times 10^{35}$  erg s $^{-1}$  and  $3.6 \times 10^{35}$  erg s $^{-1}$ , respectively. A plausible explanation for the non-detection of the bright central source is that putative binary went into a quiescent state after forming jet-structures in a past active phase.

The synchrotron cooling timescale (Reynolds 1996) for electrons which emit  $\epsilon_{\text{syn}}$  keV photons in a magnetic field  $B$  G is estimated to be,

$$\tau \approx 2000 \left( \frac{B}{10 \mu\text{G}} \right)^{-\frac{3}{2}} \left( \frac{\epsilon_{\text{syn}}}{1 \text{ keV}} \right)^{-\frac{1}{2}} \text{ years.} \quad (4)$$

Assuming the magnetic field of 100  $\mu\text{G}$  (Law et al. 2008), the cooling timescale for  $\geq 1$  keV photons is estimated to be less than  $\sim 40$ –50 years. The lower energy electrons responsible for the radio synchrotron radiation can survive much longer time. The cooling time of the X-ray emitting plasma, which are made by the interaction between the jets and the molecular clouds, is also much longer. Thus the radio Tornado and the twin X-rays at the both ends would be fossil radiations of a past activity some  $\sim 40$ –50 years ago. Although such object is very rare, we see a hint in the jets of 4U 1755–33. The central source is in low luminosity of  $3.6 \times 10^{31}$  erg s $^{-1}$  at present, but was bright two decades ago (Angelini & White 2003, Roberts et al. 1996).

### 4.4. Remnant of an Equatorial Explosion

An alternative possibility for the bipolar structure of the Tornado is a remnant of an equatorial explosion of a rotating high mass star (Shaver et al. 1985). For example, a hypernova explosion associated with a  $\gamma$ -ray burst may produce a bipolar blast wave (Ioka et al. 2004). If this blast wave hits molecular clouds, then the double X-ray spots will be produced. This scenario does not necessary require a central source. However, a hypernova is very energetic, and in our case, the explosion energy is less than  $10^{51}$  erg s $^{-1}$  (table 4). We therefore suspect this possibility is less likely compared to the bipolar-jet model of an X-ray binary.

## 5. Summary

1. We detected two diffuse X-ray sources and obtained the high quality spectra with the XIS. Both the spectra exhibit clear emission lines from highly ionized atoms, which establish the optically thin hot plasma nature. The properties of the plasmas are almost the same with each other.
2. We derived the distances to the sources by using the X-ray absorption and found that both the sources are the Galactic objects located slightly beyond the GC distance, at the consistent distance with the radio object, Tornado. Thus, together with the association in the projected image, the two X-ray sources are physically connected to the Tornado nebula.
3. The discovery of the twin thermal plasmas at the head and tail of the Tornado confirm the symmetric structure with respect to the center.
4. The most plausible origin is a bipolar jet from an accreting binary which had been active in the past and has recently entered the quiescent state. In this view, the X-ray emission is a fossil radiation from shock heated gas made by the past jet activity of the central core source. The non-thermal synchrotron X-rays may be already cooled down below the detection limit.

The authors thank all of the Suzaku team members for their full support of the Suzaku project. We acknowledge the financial support from the Ministry of Education, Culture, Sports, Science and Technology (MEXT) of Japan; the Grant-in-Aid for the Global COE Program “The Next Generation of Physics, Spun from Universality and Emergence” and others for Scientific Research B (No. 20340043 and 23340047). KK is supported by the Challenging Exploratory Research program. MS is supported by Japan Society for the Promotion of Science (JSPS) Research Fellowship for Young Scientists.

## References

- Anders, E., & Grevesse, N. 1989, *Geochim. Cosmochim. Acta*, 53, 197
- Angelini, L., & White, N. E. 2003, *ApJ*, 586, L71
- Arnaud, K. A. 1996, *Astronomical Data Analysis Software and Systems V*, 101, 17
- Bautz, M. W., Kissel, S. E., Prigozhin, G. Y., LaMarr, B., Burke, B. E., & Gregory, J. A. 2004, *Proc. SPIE*, 5501, 111
- Becker, R. H., & Helfand, D. J. 1985, *Nature*, 313, 115
- Caswell, J. L., Kesteven, M. J., Bedding, T. R., & Turtle, A. J. 1989, *Proceedings of the Astronomical Society of Australia*, 8, 184
- Dickel, J. R., Milne, D. K., Kerr, A. R., & Ables, J. G. 1973, *Australian Journal of Physics*, 26, 379
- Evans, I. N., et al. 2010, *ApJS*, 189, 37
- Frail, D. A., Goss, W. M., Reynoso, E. M., Giacani, E. B., Green, A. J., & Otrupcek, R. 1996, *AJ*, 111, 1651
- Gaensler, B. M., Fogel, J. K. J., Slane, P. O., Miller, J. M., Wijnands, R., Eikenberry, S. S., & Lewin, W. H. G. 2003, *ApJ*, 594, L35

- Helfand, D. J., & Becker, R. H. 1985, *Nature*, 313, 118  
Ioka, K., Kobayashi, S., & Mészáros, P. 2004, *ApJ*, 613, L17  
Ishisaki, Y., et al. 2007, *PASJ*, 59, S113  
Koyama, K., et al. 2007a, *PASJ*, 59, S23  
Koyama, K., et al. 2007b, *PASJ*, 59, S245  
Kundu, M. R., Velusamy, T., & Hardee, P. E. 1974, *AJ*, 79, 132  
Kushino, A., Ishisaki, Y., Morita, U., Yamasaki, N. Y., Ishida, M., Ohashi, T., & Ueda, Y. 2002, *PASJ*, 54, 327  
Law, C. J., Yusef-Zadeh, F., Cotton, W. D., & Maddalena, R. J. 2008, *ApJS*, 177, 255  
Lazendic, J. S., Wardle, M., Burton, M. G., Yusef-Zadeh, F., Green, A. J., & Whiteoak, J. B. 2004, *MNRAS*, 354, 393  
Manchester, R. N. 1987, *A&A*, 171, 205  
Miley, G. 1980, *ARA&A*, 18, 165  
Mills, B. Y., Slee, O. B., & Hill, E. R. 1960, *Australian Journal of Physics*, 13, 676  
Mitsuda, K., et al. 2007, *PASJ*, 59, S1  
Morrison, R., & McCammon, D. 1983, *ApJ*, 270, 119  
Muno, M. P., et al. 2004, *ApJ*, 613, 326  
Radhakrishnan, V., Goss, W. M., Murray, J. D., & Brooks, J. W. 1972, *ApJS*, 24, 49  
Reynolds, S. P. 1996, *ApJ*, 459, L13  
Rho, J., & Petre, R. 1998, *ApJ*, 503, L167  
Roberts, M. S. E., Michelson, P. F., Cominsky, L. R., Marshall, F. E., Corbet, R. H. D., & Smith, E. A. 1996, *IAU Circ.*, 6302, 2  
Ryu, S. G., Koyama, K., Nobukawa, M., Fukuoka, R., & Tsuru, T. G. 2009, *PASJ*, 61, 751  
Serlemitsos, P. J., et al. 2007, *PASJ*, 59, S9  
Shaver, P. A., Salter, C. J., Patnaik, A. R., van Gorkom, J. H., & Hunt, G. C. 1985, *Nature*, 313, 113  
Shull, J. M., Fesen, R. A., & Saken, J. M. 1989, *ApJ*, 346, 860  
Slee, O. B., & Dulk, G. A. 1974, *Galactic Radio Astronomy*, 60, 347  
Smith, R. K., Brickhouse, N. S., Liedahl, D. A., & Raymond, J. C. 2001, *ApJ*, 556, L91  
Stewart, R. T., Haynes, R. F., Gray, A. D., & Reich, W. 1994, *ApJ*, 432, L39  
Tawa, N., et al. 2008, *PASJ*, 60, S11  
Uchiyama, H., et al. 2009, *PASJ*, 61, S9  
Uchiyama, H., Nobukawa, M., Tsuru, T. G., Koyama, K., & Matsumoto, H. 2011, *PASJ*, submitted  
Weiler, K. W., & Panagia, N. 1980, *A&A*, 90, 269  
Yamauchi, S., & Koyama, K. 1993, *ApJ*, 404, 620  
Yusef-Zadeh, F., Goss, W. M., Roberts, D. A., Robinson, B., & Frail, D. A. 1999, *ApJ*, 527, 172  
Yusef-Zadeh, F., Wardle, M., Rho, J., & Sakano, M. 2003, *ApJ*, 585, 319